

STUDY AND PERFORMANCE OF MULTI LEVEL CASCADED SHUNT ACTIVE FILTER FOR AIRCRAFT APPLICATION

Irshad Basha Shaik, G.Naveen, M.Kondalu, S.Ananthasai

Abstract— With the progress of “more electric aircraft,” introducing active power filter (APF) technology into the aircraft power system to improve its quality and reliability catches growing interest. In this paper, based on the analysis and modeling of the shunt APF with close-loop control, a feed forward compensation path of load current is proposed to improve the dynamic performance of the APF. The two H-bridge cascaded inverter is selected for the aeronautical APF (AAPF). Justifications paper for topology choosing and corresponding system control method are given. Furthermore, the global framework and operation principle of the proposed AAPF are presented in detail. A prototype with the load power of 7.2 kVA is built and tested in the laboratory. Experimental results verify the feasibility of the proposed AAPF and the high performance of the control strategy during steady-state and dynamic operations. The increasing use of electrical power in place of hydraulic, pneumatic, and mechanical power is demanding more advanced aircraft power systems. The concept of the “all-electric aircraft” and the “more electric aircraft” (MEA) have been introduced to overcome some of the drawbacks found in conventional architectures and bring more attractive advantages, such as improved fuel consumption and lower maintenance and operation costs. This implies an increase of the electrical load and power electronic equipment, higher consumption of electrical energy, more demand for generated power, power quality, and stability problems.

Manuscript received July 15, 2014

Irshad Basha Shaik, Student Joginpally B.R Engineering College, Hyderabad, India

G.Naveen, Assoc.Prof Joginpally B.R Engineering College Hyderabad, India

M.Kondalu, Prof & Head, Joginpally B.R Engineering College, Hyderabad, India

S.Ananthasai, Asst.Prof, Joginpally B.R Engineering College Hyderabad, India

Index Terms— APF : Active Power Filter, AAPF : Aeronautical Active Power Filter, EPS: Electric Power Supply, MEA: More Electric Aircraft, CPS : Carrier Phase Shift, PWM : Pulse Width Modulation, IR: International Rectifier, THD: Total Harmonic Distortion.

I. INTRODUCTION

The latest research about civil aircraft systems has moved towards the increasing use of electric power in place of other conventional sources like mechanical, hydraulic, pneumatic power. This technological trend is known as the Electric Aircraft.

Recent advances in the areas of power electronics, electric devices, control electronics devices, and microprocessors have allowed fast improvements in the performance of a aircraft electrical systems. The use of electric power brings significant advantages for the operation of the whole system. These advantages are listed here.

Advantages of the increasing use of electric power in the aircraft system:

- optimization of the performance
- optimization of the life cycle cost
- reduction of weight and size of the equipment
- increased reliability

Important changes are brought to the aircraft electrical system due to the increasing use of electric power. These changes are listed below. Consequences of the increasing use of electric power on the aircraft electrical system:

- more electrical loads
- more complex topology of the electrical network

These aspects have to be taken into account when designing the devices in the system. It is crucial to guarantee that not only the device itself functions properly according to the specifications, but also that the interaction with the whole system respects the required conditions. In a system like the aircraft power network, the amount of generated power cannot be considered as infinite compared to the demanded power. Strict limitations are imposed on the stability and the power quality of the aircraft power system, in

of the regulator is sent to the multiplier as well as a synchronous sine wave which is detected from the phase voltage. The output of the multiplier is sent to the current regulator, being the source current reference. The output of the current regulator will be sent to the modulator to generate the pulse width modulation waveforms. Fig. 2.3 gives the equivalent control model of this compensation strategy. As shown in Fig. 2.3, the source current reference of the source current direct control comes from the variation of the dc-link voltage. Here, $G_V(s)$ corresponds to the transfer function of the voltage controller; K_f is the dc-link voltage detection coefficient.

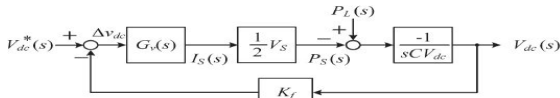


Fig. 2.2. Model for active power analysis

2.3. Load Current Feed forward Compensation

As Fig. 2.1 illustrates, load power $PL(s)$ works as a disturbance factor on the APF system. The transfer function between $PL(s)$ and $\Delta V_{dc}(s)$ is

$$\varphi_{en}(s) = \frac{\Delta V_{dc}(s)}{P_L(s)} = \frac{\frac{1}{sCV_{dc}} K_f}{1 + G_V(s) \cdot \frac{1}{2} V_s \cdot \frac{1}{sCV_{dc}} K_f} \quad (2.1)$$

The transfer function between $IL(s)$ and $IS(s)$ is

$$H_{iL}(s) = \frac{I_s^*(s)}{I_L(s)} = \frac{\Delta V_{dc}(s) G_V(s)}{P_L(s) / \frac{1}{2} V_s} + \varphi_{en}(s) \cdot \frac{G_V(s)}{\frac{1}{2} V_s}$$

$$= \frac{G_V(s) \cdot \frac{1}{2} V_s \cdot \frac{1}{sCV_{dc}} K_f}{s + G_V(s) \cdot \frac{1}{2} V_s \cdot \frac{1}{sCV_{dc}} K_f} = \frac{A \cdot G_V(s)}{s + A \cdot G_V(s)} \quad (2.2)$$

Where $A = V_s K_f / (2CV_{dc})$.

$H_{iL}(s)|_{f=50}$ shows the dynamic speed of the current reference responding to the load power's change at fundamental frequency. Generally speaking, high dynamic respond is required for an APF system, meaning that a higher value of $H_{iL}(s)|_{f=50}$ is desired. However, $H_{iL}(s)$ is sensitive to many other factors, i.e., voltage controller, line voltage, dc-link voltage, dc-link capacitor, and voltage detection coefficient. Fig. 3.4 shows the bode diagram of $H_{iL}(s)$ in different voltage controller and coefficient A. For an APF system applied in a 220-V/50-Hz application, coefficient A corresponds to 0.14 when the dc-link voltage is 800 V, dc-link voltage detection coefficient K_f is 0.005, and the dc-link capacitor is 6800 μF . It is hard to design a voltage controller to derive a high value for $H_{iL}(s)|_{f=50}$ at 50 Hz in such a low value of A. In the aircraft EPS, the phase voltage is only 115 V, leading A to be 0.2 when the dc-link voltage is 600 V, dc-link voltage detection coefficient K_f is 0.005, and the dc-link capacitor is 3300 μF . It means that poor dynamic respond is derived in both applications. In order to improve the dynamic speed responding to the load's

change, A feed forward compensation path is added to weaken the disturbance effect of the load current. Here, $F(s)$ is the transfer function of the low-pass filter (LPF) which extracts the fundamental components of the load currents.

$$F(S) = \frac{\omega_0^2}{s^2 + \sqrt{2}\omega_0 s + \omega_0^2} \quad (2.3)$$

Here, $\omega_0 = 2\pi fc$ is the cutoff angular frequency of the LPF. After the fundamental of the load current is feed forward, the transfer function between $IL(s)$ and $IS(s)$ becomes[12]

$$H_{iL}(S) = \frac{A \cdot G_V(s)}{s + A \cdot G_V(s)} + \frac{\omega_0^2}{s^2 + \sqrt{2}\omega_0 s + \omega_0^2} \quad (2.4)$$

Fig. 2.2 shows the bode diagram of $H_{iL}(s)$ with feed forward compensation and different cutoff frequencies[11]. After the load current is feed forward, the magnitude of $H_{iL}(s)|_{f=50}$ gets increased. However, the selection of fc plays an important role to $H_{iL}(s)$; usually, fc should be larger than the fundamental frequency.

III. CONTROL METHOD OF THE CASCADED-INVERTER-BASED AAPF

3.1. Discussion and Demonstration on the Power Stage of AAPF

A shunt APF acts as a controlled harmonic current source, injecting current which is inverse equivalent to the load harmonic. In the 400-Hz aircraft EPS, frequencies of the 11th and 13th harmonics reach as high as 4.4 and 5.2 kHz. How to draw a high-frequency harmonic current accurately is a key issue of developing AAPF [3].

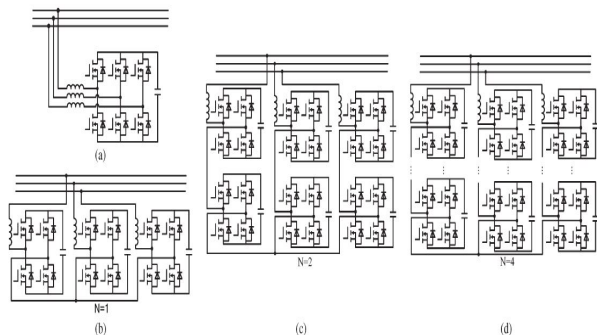


Fig. 3.1. Four possible solutions of AAPF. (a) Three-leg-inverter-based APF. (b) H-bridge-based APF. (c) Two H-bridge cascaded APF. (d) Four H-bridge cascaded APF

$$P_{con} = I_{RMS}^2 R_{ds(on)} D + V_{DF} I_D (1 - D).$$

TABLE PARAMETERS OF FOUR POSSIBLE AAPF SOLUTIONS

STUDY AND PERFORMANCE OF MULTI LEVEL CASCADED SHUNT ACTIVE FILTER FOR AIRCRAFT APPLICATION

Solution	Dc-link Voltage (V)	Switching Frequency(KHz)
Three leg inverter based APF	400	60
		120
		240
		30
H-bridge based APF	300	60
		120
Two H-bridge cascaded APF	150	30
		60
Four H-bridge cascaded APF	75	7.5
		15

Table 3.1 shows four possible solutions of APF

the three leg-inverter-based APF, the H-bridge-based APF, the two H-bridge cascaded APF, and the four H-bridge cascaded APF. Comparative study of these solutions is taken as follows. For the first solution, in order to achieve good current tracking performance in 400-Hz system, the switching frequencies of APF are selected as 30, 60, 120, and 240 kHz, and the dc-link voltage is adopted as 400 V. For the second solution, considering the “double equivalent switching frequency effect” of the carrier phase shift PWM modulation the switching frequencies of AAPF are selected as 30, 60, and 120 kHz, and the dc-link voltage is adopted as 300 V. Meanwhile, the same equivalent switching frequency means almost the same current tracking performance and almost the same bandwidth of AAPF. The switching frequencies and dc-link voltage of the other two solutions are given in Table 3.1. The power switches in Table 3.1 are all from International Rectifier (IR) Corporations with the current rating near 24 A. The switching losses and conductive losses of the power MOSFET could be evaluated by using the switching loss estimation method used .Here, P_{SW} and P_{con} correspond to switching loss and conductive loss, and ID , VD , and f_{sw} are the drain current, bus voltage, and switching frequency, while t_{ON} and t_{OFF} are the power MOSFET turn-on and turnoff times, respectively. $COSS$ $R_{ds(on)}$ are the output capacitance and the on-resistance of the power MOSFET while V_{DF} is the forward voltage drop of the reverse parallel diode of the power MOSFET. Power loss distributions of the four different AAPF solutions are given in Fig. 3.1.2.

1) Compared with the last two solutions, switching power loss plays important roles for the first two solutions. Un negligible switching power losses make the first two solutions less competitive when the switching frequency increases.
 2) Negligible switching power losses in the last two solutions make the total power losses smaller in a wide range of switching frequency. Meanwhile, power losses of the last two solutions are nearly in the same level. On the other hand, the “dead-time effect” deteriorates the current tracking performance of APF The switching frequency is selected as 30 kHz, so the ac voltage of each cluster becomes a five-level line-to neutral PWM waveform with the lowest harmonic sideband centered at 120 kHz Maintenance of the voltage balance of the capacitors is critical to the safe operation of the H-bridge-based

AAPF. The voltage-balance control of the floating dc capacitors can be divided into the following:

- 1) Clustered overall control;
- 2) Balancing control.

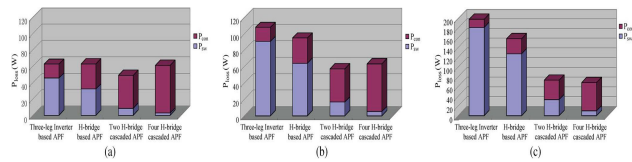


Fig. 3.1.1 Power losses of different possible AAPF solutions (a) with the equivalent switching frequency freq. of 60 kHz (b) With the equivalent switching frequency freq. of 120 kHz (c) With the equivalent switching frequency freq. of 240 kHz.

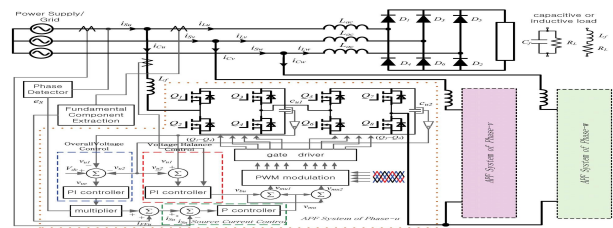


Fig. 3.1.2. System diagram of the proposed AAPF

3.2 Clustered Overall Control

In the cluster overall voltage control loop, sums of the capacitor voltages in each cluster (for example: v_{u1} and v_{u2} for phase- u) are the control target. This cluster overall control yields the u -phase clustered overall voltage signal v_{ou} from the dc capacitor voltage reference v_{dc} , the dc capacitor voltages of the u -phase cluster v_{u1} , v_{u2} , and the synchronous sine wave e_{Su} (as shown in Fig. 3.2.) The remaining cascaded units would share the dc-link voltage of the fault one.

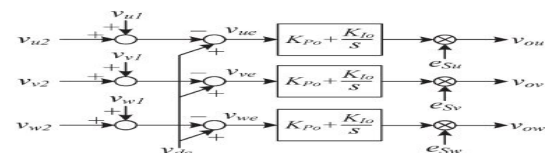


Fig. 3.2.1 Control diagram of the cluster overall control.

This voltage control scheme can increase the fault toleration and reliability of the AAPF system[5].

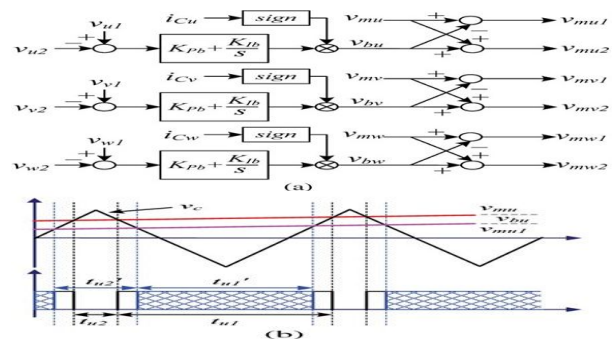


Fig. 3.2.2. Operation principle of voltage-balance control. (a) Control diagram.(b) Regulation procedure.

3.3. Balancing Control

The balancing control yields a balance control signal v_{bn} ($n = u, v, w$) to make the voltage of the capacitors in each cluster balanced. The individual balance control yields two modulation waves v_{m1} and v_{m2} from the origin modulation wave v_m and the dc capacitor voltages of each cluster v_{n1}, v_{n2} . In the CPS PWM modulation, PWM signals for Q_1, Q_2 and Q_3, Q_4 are modulated by v_{m1} , while PWM signals for Q_5, Q_6 and Q_7, Q_8 are modulated by v_{m2} as shown in fig 3.3.1. The current direction and the switch combination define the charging or discharging of the each particular capacitor of the dc link. Depending on the current direction and needed charging or discharging process, the voltage signal v should be added or subtracted to/from the modulating signal. For the upper cascaded unit, the input power decreases when the duty cycles of Q_1 and Q_4 decrease, resulting in the dc-link voltage v_{u1} being reduced. Similarly, the dc-link voltage of the lower cascaded unit v_{u2} will get increased. The voltage balance is therefore achieved. Take the phase-u cluster for example to show the regulation procedure of voltage-balance control. In the steady state, the modulation wave of bridge 1 (composed of Q_1 and Q_2) is v_{mu} , and the conduct times of Q_1 and Q_2 are t_{u1} and t_{u2} , respectively. When the situation $v_{u1} > v_{u2}$ happens, a positive balance control voltage signal v_{bu} is obtained under the regulator's action. The final modulation wave for Q_1 and Q_2 is the sum of v_{mu} and $-v_{bu}$, which becomes v_{mu1} after regulation[10]. Therefore, the conduction times of Q_1 and Q_2 turn to be t_{u1} and t_{u2} . We could find that $t_{u1} < t_{u1}$ and $t_{u2} > t_{u2}$, which means that the duty cycle of Q_1 decreased but the duty cycle of Q_2 increased[4][9]. Meanwhile, the duty cycle of Q_3 increased, and the duty cycle of Q_4 decreased.

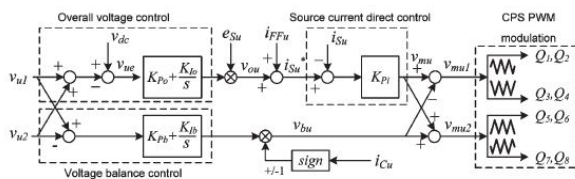
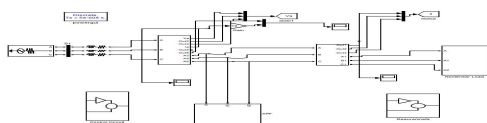


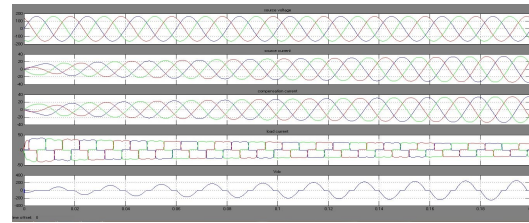
Fig. 3.3.1. Control diagram for phase-u of the proposed AAPF.

IV. MATLAB/SIMULATION RESULTS

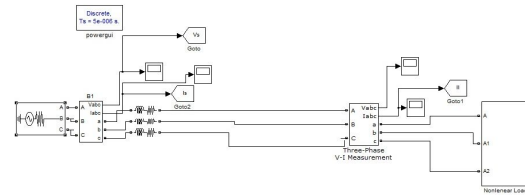
Simulation results with APF for inductive Load



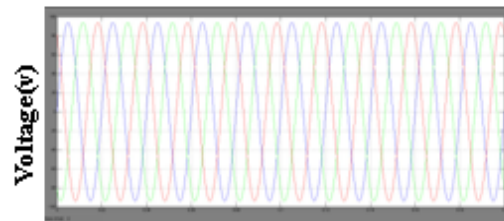
Simulated waveforms for 50-Hz EPS application with Inductive load



Simulation for without APF

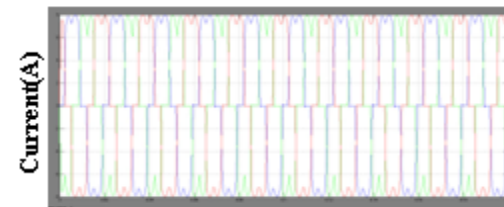


SOURCE VOLTAGE



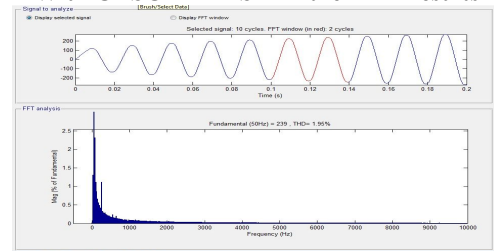
Time(sec)

LOAD CURRENT

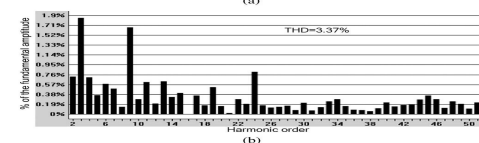
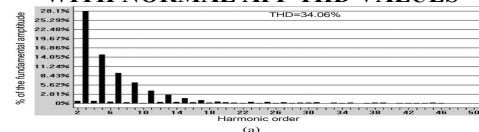


Time(sec)

With CASCADED SAPF the THD results

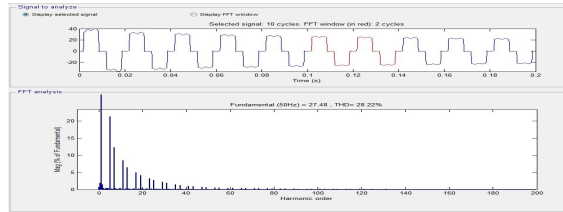


WITH NORMAL APF THD VALUES



Current THD. (a) Load current. (b) Source current.

Without APF the THD results are



V. CONCLUSION

APF technology is a useful method to resolve the power quality issues of the modern aircraft EPS. In this paper, a load current feed forward compensation method for the source current direct control-based AAPF has been proposed. The corresponding system control strategy of the cascaded-inverter based active filter system is shown. behavior for various kinds of nonlinear load condition and the excellent dynamic performance of the proposed control method

REFERENCES

1. J. A. Rosero, J. A. Ortega, E. Aldabas, and L. Romeral, "Moving towards a more electric aircraft," *IEEE Aerosp. Electron. Syst. Mag.*, vol. 22, no. 3, pp. 3–9, Mar. 2007.
2. A. Hamadi, S. Rahmani, and K. Al-Haddad, "A hybrid passive filter configuration for VAR control and harmonic compensation," *IEEE Trans. Ind. Electron.*, vol. 57, no. 7, pp. 2419–2434, Jul. 2010.
3. A. Varschavsky, J. Dixon, M. Rotella, and L. Moran, "Cascaded nine-level inverter for hybrid-series active power filter, using industrial controller," *IEEE Trans. Ind. Electron.*, vol. 57, no. 8, pp. 2761–2767, Aug. 2010.
4. A. Luo, X. Xu, L. Fang, H. Fang, J. Wu, and C. Wu, "Feedback– feedforward PI-type iterative learning control strategy for hybrid active power filter with injection circuit," *IEEE Trans. Ind. Electron.*, vol. 57, no. 11, pp. 3767–3779, Nov. 2010.
5. S. Rahmani, N. Mendalek, and K. Al-Haddad, "Experimental design of a nonlinear control technique for three-phase shunt active power filter," *IEEE Trans. Ind. Electron.*, vol. 57, no. 10, pp. 3364–3375, Oct. 2010.
6. B. Singh and J. Solanki, "An implementation of an adaptive control algorithm for a three-phase shunt active filter," *IEEE Trans. Ind. Electron.*, vol. 56, no. 8, pp. 2811–2820, Aug. 2009.
7. A. Bhattacharya and C. Chakraborty, "A shunt active power filter with enhanced performance using ANN-based predictive and adaptive controllers," *IEEE Trans. Ind. Electron.*, vol. 58, no. 2, pp. 421–428, Feb. 2011.
8. D. Ganthony and C. M. Bingham, "Integrated series active filter for aerospace flight control surface actuation," in *Proc. EPE*, 2007, pp. 1–9.
9. E. Lavopa, E. Summer, P. Zanchetta, C. Ladisa, and F. Cupertino, "Realtime estimation of fundamental frequency and harmonics for active power filters

- applications in aircraft electrical systems," in *Proc. EPE*, 2007, pp. 4220–4229.
10. E. Lavopa, M. Summer, P. Zanchetta, C. Ladisa, and F. Cupertino, "Real-time estimation of fundamental frequency and harmonics for active power filters applications in aircraft electrical systems," *IEEE Trans. Ind. Electron.*, vol. 56, no. 8, pp. 2875–2884, Aug. 2009.
11. M. Odavic, P. Zanchetta, and M. Summer, "A low switching frequency high bandwidth current control for active shunt power filter in aircrafts power networks," in *Proc. IEEE IECON*, 2007, pp. 1863–1868.
12. V. Biagini, M. Odavic, P. Zanchetta, M. Degano, and P. Bolognesi, "Improved dead beat control of a shunt active filter for aircraft power systems," in *Proc. IEEE ISIE*, 2010, pp. 2702–2707